Targeted Heating of Mitochondria Greatly Augments Nanoparticle-Mediated Cancer Chemotherapy

Jiangsheng Xu,
Fishell Department of Bioengineering, University of Maryland, College Park, MD 20742, USA

Department of Biomedical Engineering, The Ohio State University, Columbus, OH 43210, USA

Comprehensive Cancer Center, The Ohio State University, Columbus, OH 43210, USA

James G. Shamul,
Fishell Department of Bioengineering, University of Maryland, College Park, MD 20742, USA

Hai Wang,
Fishell Department of Bioengineering, University of Maryland, College Park, MD 20742, USA

Department of Biomedical Engineering, The Ohio State University, Columbus, OH 43210, USA

Comprehensive Cancer Center, The Ohio State University, Columbus, OH 43210, USA

John Lin,
Fishell Department of Bioengineering, University of Maryland, College Park, MD 20742, USA

Pranay Agarwal,
Department of Biomedical Engineering, The Ohio State University, Columbus, OH 43210, USA

Mingrui Sun,
Department of Biomedical Engineering, The Ohio State University, Columbus, OH 43210, USA

Xiongbin Lu,
Department of Medical and Molecular Genetics, Indiana University School of Medicine, Indianapolis, IN 46202, USA

Katherine H. R. Tkaczuk,
Marlene and Stewart Greenebaum Comprehensive Cancer Center, University of Maryland, Baltimore, MD 21201, USA

Xiaoming He
Fishell Department of Bioengineering, University of Maryland, College Park, MD 20742, USA

Department of Biomedical Engineering, The Ohio State University, Columbus, OH 43210, USA

Comprehensive Cancer Center, The Ohio State University, Columbus, OH 43210, USA

shawnhe@umd.edu.

Marlene and Stewart Greenebaum Comprehensive Cancer Center, University of Maryland, Baltimore, MD 21201, USA

Robert E. Fischell Institute for Biomedical Devices, University of Maryland, College Park, MD 20742, USA

Abstract

Cancer is the second leading cause of mortality globally. Various nanoparticles have been developed to improve the efficacy and safety of chemotherapy, photothermal therapy, and their combination for treating cancer. However, most of the existing nanoparticles are low in both subcellular precision and drug loading content ($<\approx5\%$), and the effect of targeted heating of subcellular organelles on the enhancement of chemotherapy has not been well explored. Here, a hybrid Py@Si-TH nanoparticle is reported to first target cancer cells overexpressed with the variant CD44 via its natural ligand HA on the outermost surface of the nanoparticle before cellular uptake, and then target mitochondria after they are taken up inside cells. In addition, the nanoparticle is ultraefficient for encapsulating doxorubicin hydrochloride (DOX) to form Py@Si-TH-DOX nanoparticle. The encapsulation efficiency is $\approx100\%$ at the commonly used low feeding ratio of 1:20 (DOX:empty nanoparticle), and $>80\%$ at an ultrahigh feeding ratio of 1:1. In combination with near infrared (NIR, 808 nm) laser irradiation, the tumor weight in the Py@Si-TH-DOX treatment group is 8.5 times less than that in the Py@Si-H-DOX (i.e., DOX-laden nanoparticles without mitochondrial targeting) group, suggesting targeted heating of mitochondria is a valuable strategy for enhancing chemotherapy to combat cancer.

Keywords

1. Introduction

Cancer is the second leading cause of death globally and chemotherapy has been used for treating many types of cancers in the clinic.[1] Unfortunately, cancer patients treated with chemotherapy often suffer from unintended deleterious side effects of chemotherapy drugs. [2] Limiting the administered drug dosage is one of the major strategies for reducing the side effects. Nonetheless, in most cases, cancer cells with reduced dosage may become drug resistant, which requires additional drug dosage to elicit a therapeutic response.[3]

Another potential strategy for reducing the side effects of chemotherapy and improve its efficacy is to deliver chemotherapy drugs using nanoparticles.[4] However, only a small part of the nanomedicine could arrive at the tumor site in vivo and much of them might enter normal organs.[4f] Therefore, it is important to limit the drug release from nanoparticles only at the tumor site before their clearance out of the body.[5] While there have been various strategies for achieving controlled release of therapeutics from nanoparticles, the use of near-infrared (NIR) light is one of the most elegant ways.[6] This is because NIR light can be generated and manipulated with well-established techniques and its absorption by biological tissues is minimal to minimize untargeted heating of normal tissues.[7] Furthermore, NIR

light-based photothermal therapy (PTT), a therapeutic procedure for destroying tumors using heat generated by NIR laser irradiation of tumors loaded with NIR-absorptive agents (e.g., gold nanoparticles), has attracted much attention because of its minimally invasive nature compared to conventional surgical resection of solid tumors.[8] Moreover, the unique physicochemical properties of nanomaterials offer the capability of achieving PTT and controlled drug release simultaneously in a single nanoplatform, which could further reduce the side effects of chemotherapy. However, the nanoparticles designed for this purpose are often low ($<\approx 5\%$) in drug loading content (LC), even though a high (more than $\approx 50\%$) encapsulation efficiency (EE) could be achieved at low feeding ratios of drug to nanomaterials. At high drug feeding ratios, both the EE and LC are often low. Low EE entails significant waste of expensive chemotherapy drugs and low LC requires many times more exogenous materials to deliver a desired dose of the encapsulated therapeutic agents, which could incur safety concern. More recently, subcellular organelle (e.g., mitochondria)-targeted PTT has been shown to enhance the killing of cancer cells by heat, compared to PTT without subcellular targeting.[9] However, the effect of subcellular organelle-targeted heating on the efficacy of chemotherapy has not been well investigated.

Inspired by the fact that mitochondria are essential subcellular organelles in charge of metabolism, apoptosis, and even drug resistance of cancer cells,[10] we hypothesize targeted PTT of mitochondria could greatly amplify the sensitivity of cancer cells to chemotherapy drugs and reduce the drug dosages needed for clinical applications. Mitochondria perform a variety of important cellular functions including the production of the largest part of cellular ATP needed for endergonic processes, such as the pumping action of the transmembrane drug efflux pumps in drug resistance cancer cells.[11] Moreover, it is commonly thought that most chemotherapies function by inducing a form of irreversible programmed cell death called apoptosis.[12] Chemotherapy-induced cancer cell apoptosis mainly proceeds via a mitochondrial apoptotic pathway. Since mitochondria are crucial in the execution of apoptosis-mediated cell death, mitochondria-directed delivery of drugs designed to trigger apoptosis and sensitize cells to chemotherapy is likely to be a promising strategy for combating cancer.[13]

In this study, we developed a polypyrrole-silica-based (Py@Si) hybrid nanoparticle for targeting not only cancer cells but also their mitochondria (Figure 1A). The former is through the binding between hyaluronic acid (HA) decorated on the nanoparticle surface and the variant CD44 overexpressed on the malignant cells.[14] After internalization in endo/lysosomes of the cells, the HA coating detaches from the nanoparticle to expose triphenylphosphonium (TPP) that has been shown to have high binding affinity with mitochondria.[15] This dual active and sequential targeting strategy allows precise control of the drug release in tumor and generate heat in mitochondria under NIR (wavelength: 808 nm) irradiation. The former could decrease the side effects of chemotherapy by minimizing the release of drugs in normal tissues, and the latter could effectively damage mitochondria to augment the efficacy of chemotherapy. Moreover, the unique design of this nanoplatform leads to ultraefficient ($\approx 100\%$) encapsulation of doxorubicin hydrochloride (DOX) because of the π–π stacking interaction between the π structure of Py and DOX. This minimizes the amount of nanomaterials needed for drug encapsulation to further reduce any possible

toxicity of the nanomaterials. Our data suggest targeted heating of mitochondria is a valuable strategy for enhancing chemotherapy to combat cancer.

2. Results and Discussion

2.1. Synthesis and Characterization of Mitochondria Targeting Nanoparticles

The multifunctional nanoparticle is synthesized using polypyrrole (Py, a conductive polymer) and mesoporous silica, and further modified with TPP and HA sequentially on the surface. Comparing to other NIR-responsive materials (e.g., magnetic iron oxide particles[16] and gold nanomaterials[17]), Py is excellent for generating hyperthermia to treat cancer.[18] This is because they have strong absorbance of NIR (Figure 1B), great stability in physiological condition even after NIR irradiation, and a clear chemical structure and synthesis route. As illustrated in Figure 1B,C, Py was embedded in a silica matrix to form the Py@Si nanoparticle by using a reverse-microemulsion method.[2b] After modifying the surface by adding amino groups using (3-aminopropyl) trimethoxysilane (APTMS) to form Py@Si-NH$_2$ nanoparticle, TPP (its ^{1}H NMR spectrum is shown in Figure 1B) was conjugated onto the Py@Si-NH$_2$ nanoparticle through the EDC/sulfo-NHS chemical reaction to produce the mitochondria-targeting (Py@Si-T, T for TPP) nanoparticle. Lastly, the Py@Si-T nanoparticle was further coated with HA via electrostatic interaction (TPP and HA are positively and negatively charged, respectively) to produce the dual (active)-targeting (Py@Si-TH, H for HA) nanoparticles. The resultant Py@Si, Py@Si-NH$_2$, Py@Si-T, and Py@Si-TH nanoparticles were characterized by transmission electron microscopy (TEM), scanning electron microscopy (SEM), and dynamic light scattering (DLS, for both size and surface zeta potential). As shown in Figures 1C and Figure S1, Supporting Information, the Py@Si-TH nanoparticles have a core-shell and spherical morphology and are ≈75 nm in diameter. The zeta potential data of the four nanoparticles indicate successful surface modification step by step. The zeta potential of Py@Si nanoparticles at room temperature is negative (−22.0 ± 1.0 mV), while the zeta potential of Py@Si-NH$_2$ nanoparticles is positive (29.4 ± 2.9 mV) because of the primary amino group on the surface after APTMS modification. After modifying the Py@Si-NH$_2$ nanoparticles with TPP (a positively charged lipophilic mitochondria-targeting molecule), the zeta potential of the resultant Py@Si-T nanoparticles is even more positive (54.3 ± 9.6 mV). After coating with HA, the zeta potential of the resultant Py@Si-TH nanoparticles is negative (−13.3 ± 1.4 mV; Figure 1C). The HA coating on the surface of the Py@Si-TH nanoparticles after negative staining is observable with TEM (Figure 1D). Importantly, this HA coating renders good stability to the Py@Si-TH nanoparticles in aqueous suspension comparing to Py@Si-T nanoparticles. This is probably because the HA coating covers the lipophilic TPP on the surface, preventing potential aggregation of Py@Si-T nanoparticles (Figures S1 and S2, Supporting Information).

As the exposure of TPP is essential for mitochondria targeting inside cells, the detachment of HA from the outermost surface of Py@Si-TH nanoparticles under acidic condition was investigated. After incubating Py@Si-TH nanoparticles in acetate buffer at pH 5.0 (the pH value in endo/lysosomes) for 30 min, the zeta potential of the recovered nanoparticles in deionized (DI) water at pH 7.4 is positive (32.1 ± 7.4 mV; Figure 1E). This confirms that the

HA decorated on the outermost surface could detach from the nanoparticles in endo/
lysosomes with a low pH microenvironment, to expose the TPP for targeting mitochondria.
Interestingly, after incubating the Py@Si-TH nanoparticles with hyaluronidase (HAase, 5
mM) at 37 °C for 30 min at pH 7.4, the zeta potential of the recovered nanoparticles is also
positive (24.5 ± 8.7 mV; Figure 1E). This is because the HAase can degrade HA into low
molecular weight HA and monosaccharides with high solubility in water,[19] and the
resultant molecules leave the nanoparticle surface and dissolve in water to expose the
positively charged TPP on the nanoparticle surface. This data further confirm successful
decoration of HA on the Py@Si-T nanoparticles to form the Py@Si-TH nanoparticles.
Moreover, it appears that the low pH 5.0 is even more effective than the 5 mM HAase to
expose TPP on the nanoparticles on average in terms of zeta potential (32.1 ± 7.4 mV vs
24.5 ± 8.7 mV), although the difference is not statistically significant. The surface zeta
potential of the Py@Si-TH nanoparticles after the acidic and enzymatic treatments is less
than that (54.3 ± 9.6 mV) of Py@Si-T nanoparticles, indicating partial detachment/
degradation of the HA on the nanoparticle surface. It is worth noting that at pH 6, the zeta
potential of the Py@Si-TH nanoparticles remains negative (−10.9 ± 4.3; Figure S3,
Supporting Information). This ensures HA on the surface of the nanoparticles for CD44
targeting in tumor.

The Py@Si-TH nanoparticles can be used to encapsulate DOX, a widely clinically used
chemotherapy drug, in an ultraefficient manner at not only low but also high feeding ratios
of drug to empty nanoparticles (Figure 1F, top). After simply mixing the solution of DOX
with the Py@Si-TH nanoparticles for 1 h, ≈100% of the DOX could be encapsulated in the
nanoparticles when the feeding ratio is from 1:50 to 1:5 (DOX:empty nanoparticles), and
this does not change the morphology or size of the nanoparticles (Figure S4A, Supporting
Information). Interestingly, even though we increased the drug feeding ratio to an unusually
high value of 1:1, the EE is still as high as 81% (Figure 1F, top) leading to a drug loading
content of as high as ≈45% in the resultant nanoparticles. This high EE at the high drug
feeding ratio is confirmed by the minimal red appearance in the supernatant (Figure 1F,
bottom), which was made by centrifuging the free DOX solution that was incubated with the
Py@Si-TH nanoparticles for 1 h at room temperature. The advantages of this ultraefficient
encapsulation, especially at high feeding ratio, would be to dramatically enhance the LC and
to avoid the significant waste of expensive chemotherapy drugs. This could minimize the
usage of exogenous materials and reduce their potential side effects (if any). We used a
feeding ratio (DOX:nanoparticle) of 1:10 for further in vitro and in vivo studies. This ratio
was used to achieve maximum EE of DOX (≈100%), high loading content (≈10%), and a
target bulk tumor tissue temperature of <50 °C (to minimize thermal damage to the normal
tissue[20]). In addition, the resultant DOX-laden nanoparticles (Py@Si-TH-DOX) are stable
in cell culture medium, as indicated by their diameter (74.8 ± 6.9 nm) after 12 h of
incubation in the cell culture medium at 37 °C (Figure S4B, Supporting Information). This
observation is further confirmed by incubating the Py@Si-TH-DOX nanoparticles in human
blood serum at 37 °C for 12 h to measure their diameter (70.7 ± 18.4 nm, Figure S5A,
Supporting Information). In contrast, the diameter of the Py@Si-T-DOX nanoparticles
without HA on their surface increases to 577.4 ± 254.6 nm after incubated in human blood

serum at 37 °C for 12 h (Figure S5B, Supporting Information). These data indicate the HA decoration is important to ensure the nanoparticle stability under physiological condition.

2.2. Photothermal Effect of Nanoparticles

We then investigated the photothermal effect of the Py@Si-TH nanoparticles in phosphate buffered saline (PBS) (pH 7.4). Upon irradiation with NIR laser at 1.0 W cm^{-2} for 5 min, the temperature of the aqueous nanoparticle suspension (30 μg mL^{-1}) increases by ≈12 °C while the change in temperature in the control group (PBS only) is much less (≈1.5 °C; Figure 2A). Although a similar photothermal effect can be achieved with 5 μg mL^{-1} indocyanine green (ICG, another commonly used NIR photosensitizer[2b,7c]) in PBS, the temperature change reaches a plateau after 5 min of NIR irradiation due to the photobleaching effect of NIR laser on ICG as a small organic fluorescence molecule. In contrast, the temperature keeps increasing in the aqueous suspension of the Py@Si-TH nanoparticles with further heating to 10 min. Moreover, the photothermal effect of the Py@Si-TH nanoparticles is highly stable compared with that of ICG. As shown in Figure 2B, the photothermal effect of the nanoparticles remains almost the same within five cycles of NIR laser irradiation while it decays for ICG after every cycle of the NIR irradiation. In addition, the photothermal effect of the Py@Si-TH nanoparticles is laser dose dependent. As shown in Figure 2C, the increase of temperature in the aqueous nanoparticle suspension is faster when the laser power increases from 0.5 to 1.0 W cm^{-2}.

Next, we investigated the photothermal effect of the Py@Si-TH nanoparticles inside cells, for which the MDA-MB-231 human triple negative breast cancer cells were incubated with the nanoparticles (30 μg mL^{-1}) at 37 °C for 4 h. After the treatment, the medium with nanoparticles were replaced with room-temperature pure medium. The cells attached on Petri dish in pure medium were then irradiated with NIR laser and the temperature of the cells was monitored by using a FLIR (Wilsonville, OR, USA) E6 infrared thermal camera (see Figure 2D for a schematic illustration). As shown in Figure 2E, the temperature in the area with NIR laser irradiation increases by ≈6.5 and 10.5 °C after 1 min and 4 min of continuous irradiation, respectively. By contrast, the change of temperature is minimal in the area of NIR laser irradiation if the cells are not treated with the nanoparticles. These data demonstrated that the photothermal effect of the Py@Si-TH nanoparticles maintains after they are taken up inside cells.

To confirm that mitochondria targeted Py@Si-TH nanoparticles are more efficient to induce cell death by hyperthermia than non-mitochondria targeting nanoparticles, we investigated the viability of MDA-MB-231 cells loaded with Py@Si-H and Py@Si-TH nanoparticles upon NIR laser irradiation. The Py@Si-H nanoparticles were made by coating HA on the Py@Si-NH$_2$ nanoparticles via electrostatic interaction. They do not have the mitochondria-targeting TPP but have similar size, surface zeta potential, and spherical morphology to the Py@Si-TH nanoparticles (Figure S6, Supporting Information). Cell uptake of the nanoparticles was done by incubating the cells and the different nanoparticles in the same way as aforementioned and the nanoparticle-containing medium was replaced with pure medium at 37 °C before laser irradiation at 1.0 W cm^{-2} for 1 or 2 min. Afterward, the cells were incubated at 37 °C for 6 h. The live and dead cells were then stained with calcein AM

(green) and propidium iodide (PI, red), respectively, for their visualization (Figure 2D). The qualitative fluorescence images showing the cell viability and the corresponding quantitative data are shown in Figure 2F. First of all, the NIR laser irradiation alone does not induce appreciable cytotoxicity to the cells without nanoparticle treatment (i.e., treated with PBS). Similarly, the nanoparticle treatment alone (i.e., 0 min of NIR irradiation) does not induce any significant cell death. Importantly, with NIR laser irradiation, significantly and many more dead cells can be observed for the treatments with the mitochondria-targeting Py@Si-TH nanoparticles, than the treatment with Py@Si-H nanoparticles that do not have mitochondria-targeting capability. These data suggest that precise targeting of the subcellular organelle mitochondria can greatly sensitize cancer cells to PTT.

2.3. Mitochondria-Targeting Capability of Py@Si-TH-DOX Nanoparticles and NIR Controlled Release of DOX

To investigate the mitochondria targeting capability of the Py@Si-TH-DOX nanoparticles, we stained mitochondria using MitoTracker Deep Red for visualization using confocal fluorescence microscopy. The confocal images were further quantitatively analyzed for colocalization of DOX with nuclei and mitochondria using Manders' coefficients M1 (b–g) (the fraction of blue/nuclei overlapping with green/DOX), M2 (g–b) (the fraction of green/DOX overlapping with blue/nuclei), M3 (g–r) (the fraction of green/DOX overlapping with red/mitochondria), and M4 (r–g) (the fraction of red/mitochondria overlapping with green/DOX). As shown in Figure 3, free DOX (without any nanoparticle encapsulation, emission at 550–600 nm, pseudo-color green in this panel to differ it from MitoTracker Deep Red with emission at 650–670 nm) mainly accumulates in the cell nuclei due to its high binding affinity with the nuclear materials. The M1 and M2 are close to 1, indicating nearly perfect colocalization between free DOX and nuclei. On the other hand, M3 and M4 are nearly 0, indicating minimal colocalization between free DOX and mitochondria. In contrast, the red fluorescence stain of mitochondria largely overlaps with Py@Si-TH-DOX nanoparticles (green) to give the brownish color in the merged view with both M3 and M4 being close to 1, indicating the excellent capability of the Py@Si-TH-DOX nanoparticles in targeting mitochondria. This is not observed between the red fluorescence stain of mitochondria and Py@Si-H-DOX nanoparticles (with no mitochondria targeting capability), for which the M3 and M4 are much less than 1. The M1 and M2 for both the Py@Si-TH-DOX and Py@Si-H-DOX nanoparticles are nearly 0, indicating negligible colocalization between the nanoparticle-encapsulated DOX and nuclei. The latter is due to minimal release of DOX from the nanoparticles. It is worth noting that besides its high binding affinity with mitochondria, TPP has been shown to facilitate the endo/lysosomal escape of nanoparticles inside cells to make mitochondria-targeting possible.[21]

To study NIR laser irradiation-controlled drug release from Py@Si-TH-DOX nanoparticles, we investigated the release of DOX from the Py@Si-TH-DOX nanoparticles at 37 °C in aqueous solution first. Without NIR laser irradiation, the release of DOX is very slow and slightly dependent on the pH of the aqueous solution (Figure S7, Supporting Information). In contrast, the NIR laser irradiation (1.0 W cm^{-2} for 1 min) could induce a burst release of DOX out of the nanoparticles and this burst release is more evident at lower pH. Importantly, this NIR laser irradiation-triggered release of DOX from the nanoparticles retains after the

nanoparticles are taken up inside cells. As shown in Figure 3, with NIR laser irradiation at 1.0 W cm^{-2} for 2 min (Py@Si-TH-DOX+L), DOX is released from the nanoparticles and enters the cell nuclei. As a result, the M1 and M2 for the colocalization of DOX and nuclei increase and the M3 showing the fraction of DOX overlapping with mitochondria decreases, compared to the condition of Py@Si-TH-DOX (without laser irradiation). This indicates that DOX (green) release from nanoparticles in mitochondria (red) and bind with nuclei (blue) after the NIR laser irradiation. However, the M4 showing the fraction of mitochondria overlapping with DOX is nearly 1, indicating DOX still presents in nearly all mitochondria. This is probably because DOX is not completely released from the nanoparticles and the released DOX could bind with the mitochondrial DNA. In addition, the cells with the Py@Si-TH-DOX+L treatment become shrunk, probably as a result of the heat generated by the Py@Si-TH nanoparticles under the NIR laser irradiation.

2.4. Photothermally Induced Mitochondrial Damage Due to Targeted Heating of the Subcellular Organelle

Damage to mitochondria may lead to the depolarization of mitochondria and a drop in membrane potential (Ψ), which is an important indicator for evaluating mitochondrial dysfunction. In this study, the JC-1 (5,5′,6,6′-tetrachloro-1,1′,3,3′-tetrethyl benzimidazolylcarbocyanine iodide) dye was used to monitor the mitochondrial membrane potential based on the shift of its fluorescence emission. Healthy cells with high mitochondrial membrane potential promote the accumulation of the dye in their mitochondria to form the dye aggregates (J-Aggr), which gives red fluorescence. On the other hand, cells with low mitochondrial membrane potential should have very little accumulation of the dye in their mitochondria and contain mainly JC-1 monomers (J-Mono) which fluoresces green. First, we investigated the sensitivity of cancer cells to mitochondria-targeting PTT. As shown in Figure 4A, the JC-1 assay shows that cells treated with Py@Si-TH+L had brighter green fluorescence than the Py@Si-H+L (without mitochondria targeting capability) group, indicating enhanced mitochondrial damage with the mitochondria targeting Py@Si-TH nanoparticles under NIR laser irradiation.

To further confirm that mitochondria damage was induced by targeted hyperthermia, we performed experiments to quantify the real-time extracellular acidification rate (ECAR) for assessing the extent of glycolysis in cells. For this, MDA-MB-231 cells with no treatment (control) and after treatment with Py@Si-TH nanoparticles, Py@Si-TH nanoparticles with laser irradiation (Py@Si-TH+L), Py@Si-TH-DOX nanoparticles, and Py@Si-TH-DOX+L in glucose-depleted medium were studied using a Seahorse XF24 Extracellular Flux Analyzer.[22] The effective DOX concentration for all the conditions with DOX is 3 μg mL^{-1} and the nanoparticle concentration is 30 μg mL^{-1}. As shown in Figure 4B,C, glycolytic parameters were calculated by monitoring ECAR changes in response to the sequential addition of excess glucose (10 mM, for inducing glycolysis in cytoplasm), oligomycin (1.0 μM, for inhibiting oxidative phosphorylation in mitochondria and further induce the glycolytic activity), and 2-deoxy-D-glucose (2-DG; 50 mM, to compete with glucose and reduce both glycolysis and oxidative phosphorylation). The change of ECAR after adding glucose reflects the extent of glycolysis in the cells. The further change in ECAR after adding oligomycin reflects the glycolytic reserve, which is a parameter to reflect

mitochondrial function. The summation of glycolysis and glycolytic reserve is called glycolytic capacity. Administration of excess glucose to Py@Si-TH nanoparticle-treated MDA-MB-231 cells in glucose-depleted medium does not appear to impact the ECAR level much compared with the control group, although the combination of the nanoparticles and NIR laser irradiation significantly decreases the ECAR level outside the cells. Similarly, the combination of Py@Si-TH-DOX nanoparticles and NIR laser can decrease the ECAR level significantly more than the nanoparticles alone. These data indicate that treatment with NIR laser irradiation results in the significantly lower levels of ECAR or glycolysis (Figure 4C). This is probably due to the decreased supply of ATP and deactivation of hexokinases (HKs) for glycolysis after mitochondria-targeted hyperthermia. Generally, cancer cells exhibit increased glycolysis: the Warburg effect.[23] The first step of glycolysis is to trap glucose within the cell with a phosphate addition reaction using ATP to produce glucose-6-phosphate (G6P).[23] HKs is the gateway enzyme of glucose metabolism comprising of four isoforms (HK1-HK4). HK1 and HK2 are the most abundant isoforms localizing on the mitochondrial membrane and could be inactivated after the mitochondria-targeted hyperthermia to reduce glycolysis in cancer cells.[24]

2.5. Targeted Heating of Mitochondria Enhances the Sensitivity of Cancer Cells to Nanoparticle-Mediated Chemotherapy In Vitro

To investigate the anticancer capacity of Py@Si-TH-DOX nanoparticles in vitro, MDA-MB-231 cells were incubated with free DOX, Py@Si-TH nanoparticles, Py@Si-H-DOX nanoparticles (no TPP for mitochondria targeting), and Py@Si-TH-DOX nanoparticles, respectively, either with or without NIR laser irradiation at 1 W cm^{-2} for 2 min. As shown in Figure 4D, the Py@Si-TH nanoparticles without DOX or NIR irradiation are not harmful to the cells, suggesting the minimal cytotoxicity of the blank/empty nanoparticles. As expected, the toxicity of Py@Si-TH nanoparticles with either NIR laser irradiation (i.e., Py@Si-TH +L) or DOX (i.e., Py@Si-TH-DOX) to MDA-MB-231 cells is significantly increased for any given nanoparticle/DOX concentration. Interestingly, the Py@Si-TH-DOX treatment is also significantly more toxic to the cells than the Py@Si-H-DOX treatment with no mitochondria targeting capability for a given DOX/nanoparticle concentration. Although combining NIR laser irradiation with the Py@Si-H-DOX nanoparticles (i.e., Py@Si-H-DOX+L) could enhance killing of the cancer cells compared to the nanoparticles alone, the Py@Si-TH-DOX+L treatment gives significantly better anticancer effect than all the other treatments for all the DOX/nanoparticle concentrations. These data indicate targeted heating of mitochondria greatly enhances the sensitivity of cancer cells to the nanoparticle-mediated chemotherapy in vitro.

2.6. Targeted Heating of Mitochondria Enhances the Antitumor Efficacy of Nanoparticle-Mediated Chemotherapy In Vivo

To study the tumor targeting capability in vivo using in vivo imaging, we encapsulated a near infrared fluorescence dye (indocyanine green or ICG in short) in the Py@Si-TH nanoparticles to obtain Py@Si-TH-ICG nanoparticles for injection into mice bearing MDA-MB-231 xenograft tumor through the tail vein (Figure 5A). In addition, free ICG at the same dose and saline were used as control groups. As shown in Figure 5B, at 2 h after intravenous (i.v.) injection, the ICG fluorescence is visible throughout the entire body of the mouse. The

fluorescence in the tumor area is elevated in mice treated with nanoparticles at 8 h after the i.v. injection, and remains high even at 24 h after the injection, indicating preferential accumulation of the Py@Si-TH-ICG nanoparticles in the tumor. This might be due to the enhanced permeability and retention (EPR) effect of the tumor vasculature that is highly permeable to nanoparticles of 20–150 nm,[4d,25] and the capability of the nanoparticles to bind with the cancer cells in tumor via the HA-CD44 interaction.[7c,14b] Although the EPR effect might not be as evident in the tumors of human patients, nanoparticles have been shown to extravasate into tumor via active transcytosis across the endothelial cells lining the tumor vasculature.[26] In contrast, very weak ICG fluorescence signal can be detected in the tumor of the mice treated with free ICG at 8 h and it becomes not detectable at 24 h after injection. After in vivo imaging at 24 h, the mice were sacrificed and five major organs (heart, liver, spleen, lung, and kidney) together with the tumor were harvested from all the mice for ex vivo imaging to check the nanoparticle distribution. Only tumor from the Py@Si-TH-ICG group has strong fluorescence of ICG (Figure 5B). Although strong ICG fluorescence can be observed in the liver and kidney of the mice treated with the Py@Si-TH-ICG nanoparticles, the release of the encapsulated agent from the nanoparticles is minimal without NIR laser irradiation (Figure S6, Supporting Information). This mitigates the concern on their potential toxicity to normal organs. It is also worth noting that the DOX released or freed out of the nanoparticles in tumors should enter tumor cells quickly and bind with their DNA with very high affinity (see free DOX in Figure 3). Therefore, DOX in biofluids in vivo is expected to be minimal.

We next investigated the in vivo photothermal effect of the Py@Si-TH-DOX nanoparticles in MDA-MB-231 tumor-bearing mice. As shown in Figure 5A, the tumors were irradiated with NIR laser at 1.0 W cm^{-2} for 1 min at 8 h and 24 h, respectively, after i.v. injection of the nanoparticles. The temperature in the tumor was monitored using a FLIR E6 infrared thermal camera. The tumor area temperature for mice injected with Py@Si-TH-DOX nanoparticles increases by ≈10–12 °C (at both 8 and 24 h after injection) within 1 min under the NIR laser irradiation (Figure 5C), while the temperature increase for mice injected with saline or free DOX is ≈4 °C. These data further support that the Py@Si-TH-DOX nanoparticles can preferentially accumulate in tumor and specifically generate heat in tumor under NIR laser irradiation in vivo.

To test our hypothesis that targeted heating of mitochondria enhances the antitumor efficacy of nanoparticle-mediated chemotherapy in vivo, we treated tumor-bearing mice with different drug formulations to understand the safety and efficacy of the Py@Si-TH-DOX nanoparticle-mediated combination therapy of chemotherapy and PTT. As shown in Figure 5D–G, the tumor growth is not significantly different for the saline, free DOX with NIR laser irradiation (free DOX+L), Py@Si-TH nanoparticles, and Py@Si-TH-DOX nanoparticles. The low antitumor effect of the Py@Si-TH-DOX treatment (absent of NIR irradiation) was probably due to the minimal drug release from the nanoparticles. The growth of tumors in mice treated with the Py@Si-TH nanoparticles (without DOX) and NIR laser irradiation (Py@Si-TH+L) is significantly reduced compared to the Py@Si-TH treatment alone, suggesting the antitumor effect of the nanoparticle-mediated PTT. By encapsulating DOX in the nanoparticles and combining it with NIR laser irradiation (i.e., the Py@Si-TH-DOX+L treatment), the tumor growth is further significantly and greatly reduced

with complete destruction of tumors in two of the seven mice (Figure 5E). Further histological analyses (hematoxylin and eosin or H&E staining) reveal extensive necrosis in the tumors with the Py@Si-TH-DOX+L treatment compared with all the other treatments (Figure 5F).

Interestingly, the combination of Py@Si-H-DOX nanoparticles (with no mitochondria targeting capability) and NIR laser irradiation (i.e., the Py@Si-H-DOX+L treatment) is not as effective as the Py@Si-TH-DOX+L treatment: the weight of tumors from the Py@Si-H-DOX+L group is ≈8.5 times more than that from the Py@Si-TH-DOX+L group on average (Figure 5G). In view of the fact that the Py@Si-TH-DOX nanoaprticles (capable of mitochondria targeting) alone is not effective for destroying tumor, these data indicate that targeted heating of mitochondria greatly and significantly enhances the in vivo antitumor efficacy of the nanoparticle-mediated chemotherapy. Importantly, no obvious side effect was noticed during the in vivo experiments. Neither significant drop of body weight nor death was observed for the mice in all the groups (Figure 5H). No appreciable damage to the major organs was observed according to the H&E-stained slices of the organs (Figure 5I). This can be attributed to the minimal toxicity of the nanoparticles synthesized in this study and the low dosage of DOX administered (2.5 mg kg^{-1} body weight). Taken together, these data indicate the superior safety and efficacy of the mitochondria-targeting Py@Si-TH nanoparticle-mediated PTT and chemotherapy for killing tumors.

3. Conclusions

In summary, we demonstrate the ability to augment the effectiveness of chemotherapy using non-toxic, triple (passive for tumor and active for cancer cells and and mitochondria) targeting Py@Si-TH-DOX nanoparticles in combination with NIR laser irradiation. By embedding polypyrrole (Py) inside silica and decorating on the surface sequentially with TPP and HA, we fabricated a nanostructure with superb anticancer effect through precisely targeted heating of the mitochondria of cancer cells upon NIR laser irradiation. In addition, the nanoparticle is ultraefficient for encapsulating DOX because of the π–π stacking interaction between Py and DOX. The EE is ≈100% at the commonly used low feeding ratio (in weight) of 1:20 (DOX:nanoparticle), and >80% at an ultrahigh feeding ratio of 1:1. Upon NIR laser irradiation, the temperature of both in vitro cancer cells and in vivo tumors loaded with Py@Si-TH nanoparticles can be elevated by ≈10 °C within 1 min for mild hyperthermia. When combined with NIR laser irradiation, our Py@Si-TH-DOX nanoplatform can reduce tumor weight by 8.5 times compared to the Py@Si-H-DOX nanoplatform that is devoid of TPP, indicating the crucial role of the mitochondria-targeted heating for enhancing nanoparticle-mediated chemotherapy. This study suggests that targeted heating of subcellular organelles (e.g., mitochondria) is a valuable strategy to enhance cancer chemotherapy.

4. Experimental Section

Materials:

Pyrrole, cyclohexane, hexanol, tetraethyl orthosilicate (TEOS), Triton X-100, (3-Aminopropyl)triethoxysilane (APTMS), indocyanine green (ICG), and polyvinyl alcohol

(PVA) were obtained from Sigma-Aldrich (St. Louis, MO, USA). DOX was purchased from LC laboratories (Woburn, MA, USA). The CCK-8 cell proliferation reagent kit was purchased from Dojindo Molecular Technologies (Rockville, MD, USA). Fetal bovine serum (FBS) and penicillin/streptomycin were purchased from Invitrogen (Carlsbad, CA, USA). The DMEM cell culture medium was obtained from ATCC (Manassas, VA, USA). All other chemicals were purchased from Sigma unless specifically mentioned otherwise.

Synthesis of Nanoparticles:

Polypyrrole (Py) conductive polymer was synthesized according to the previous literature, [27] and was further encapsulated inside silica nanoparticles by a modified reverse microemulsion method. First, Triton X-100 (2 mL), hexanol (10 mL), and cyclohexane (2.4 mL) were mixed together for 30 min. A total of 600 μL of Py in DI water (5 mg mL^{-1}) was then added into the mixture and stirred at room temperature for 1 h. Afterward, 120 μL of ammonium hydroxide (28 wt%) and 200 μL of TEOS were added consecutively and the sample was stirred at room temperature for 24 h to form the Py-embedded silica (Py@Si) nanoparticles. Then, 40 μL of APTMS and 10 μL of TEOS were added into the sample and it was stirred overnight. Last, the sample was added into 30 mL of ethanol to terminate the reaction. The resultant Py@Si-NH$_2$ nanoparticles were cleaned and collected by centrifuging at 13 000 × g for 10 min and washing with ethanol and DI water for three times, respectively. To further modify the nanoparticles, the mitochondria-targeting ligand TPP-COOH ((3-carboxyethyl)triphenylphosphonium bromide was prepared according to a previously reported procedure.[7a] Then, 167 mg of the TPP-COOH was treated with EDC·HCl (120 mg) and sulfo-NHS (120 mg) in 5 mL of DMSO and stirred at room temperature for 1 h before being added in to the colloidal solution of Py@Si-NH$_2$ (150 mg) in 15 mL of DI water and 30 μL of triethylamine (TEA). The mixture was stirred at room temperature for 24 h and the resultant Py@Si-T nanoparticles were cleaned and collected by centrifuging at 13 000 × g for 10 min and washed with ethanol and DI water three times, respectively. Finally, the Py@Si-TH nanoparticle was synthesized by mixing the Py@Si-T nanoparticles (5 mg mL^{-1}) with HA (1 mg mL^{-1}) and stirring at room temperature for 3 h, and collected by centrifuging at 13 000 × g for 10 min. The Py@Si-H nanoparticles were synthesized in the same way using Py@Si-NH$_2$ instead of Py@Si-T nanoparticles.

Encapsulation and Release of DOX:

DOX-laden nanoparticles were made by mixing DOX and empty nanoparticles at various ratios in weight. The ratio of 1:10 (DOX:empty nanoparticles) was used for cell and animal studies because it allowed maximum EE, high LC, and a target bulk tumor tissue temperature <50 °C to minimize damage to the surrounding normal tissue by heat dissipation.

The EE and LC of DOX was calculated using the following equations:

$$EE = W_{Encap}/W_{Fed} \times 100\% \qquad (1)$$

$$LC = W_{Encap}/W_{Total} \times 100\% \qquad (2)$$

where W_{Encap} represents the measured weight of DOX encapsulated in the nanoparticles, W_{Fed} is the total amount of DOX initially included in the DOX-nanoparticle mixture for encapsulation, and W_{Total} is the total amount of agent-laden nanoparticles including both DOX and empty nanoparticles. The amount of DOX was measured using a Beckman Coulter (Indianapolis, IN, USA) DU 800 UV-Vis spectrophotometer at its 488 nm absorbance peak.

NIR laser-induced drug release was measured by collecting the supernatant of the nanoparticle suspension post-centrifugation at $13\,000 \times g$ and measuring the absorbance at 488 nm of the supernatant using UV-Vis spectrophotometry.

Characterization of Nanoparticles:

The nanoparticle size and zeta potential were measured by dispersing the nanoparticles at 1 mg mL^{-1} in DI water for DLS analysis using a Brookhaven 90 Plus/BI-MAS Particle Analyzer (Holtsville, NY, USA). The morphology of nanoparticles was imaged using both the FEI Tecnai G2 Spirit TEM and NOVA Nano400 SEM. For TEM studies, nanoparticles were examined either directly or after being negatively stained with uranyl acetate solution (2 wt%). For SEM studies, nanoparticles were sputter-coated with a thin film of Au before imaging.

Cancer Cell Culture:

Human triple negative breast cancer MDA-MB-231 cells (ATCC, Manassas, VA, USA) were cultured in Dulbecco's Modified Eagle Medium (DMEM) supplemented with 10% FBS and 1% penicillin/streptomycin at 37 °C in a 5% CO_2 incubator.

Photothermal Effect:

To investigate the photothermal conversion effect in pH 7.4 PBS, the samples were irradiated by the 808 nm NIR laser at a power density of 1.0 W cm^{-2}. The temperature changes of the solution were monitored with an Omega 5SRTC-KK-K-30–36 thermocouple (Omega Engineering, Norwalk, CT, USA). All the experiments were conducted at room temperature. To study the intracellular photothermal effect, MDA-MB-231 cells in 35 mm culture dishes were incubated with medium with or without Py@Si-H or Py@Si-TH nanoparticles (30 μg mL^{-1}) for 4 h. Next, the cells were washed with pure medium for three times. The cells were then subject to the 808 nm laser irradiation (at 1.0 W cm^{-2}) for up to 4 min. During the exposure to a laser, a time series of thermographic images were captured with a FLIR (Wilsonville, Oregon, USA) E6 thermal camera at a time interval of 10 s over 4 min. The temperature of the MDA-MB-231 cells was calculated using the FLIR R&D software.

Monitoring Cell Death Due to Hyperthermia:

MDA-MB-231 cells were seeded on 35 mm dishes at 0.5 million cells mL^{-1} in 2 mL medium for 24 h. The cells were then treated with 30 μg mL^{-1} Py@Si-H and Py@Si-TH nanoparticles, respectively, for 4 h and washed with fresh medium twice. Then, the cells were irradiated with an 808 nm NIR laser at 1.0 W cm^{-2} for 1 or 2 min. After incubation for another 6 h, the live/dead cells were fluorescently visualized by using calcein AM (green) and propidium iodide (PI; red) staining.

Imaging of Colocalization:

Subcellular imaging was performed via confocal microscopy. At 24 h before imaging, MDA-MB-231 cells were seeded onto collagen-coated Nunc (Thermo Fisher. Waltham, MA, USA) cover glass slides inside 35 mm culture dishes. Cells were then washed with culture medium and incubated in medium containing nanoparticles at an equivalent DOX concentration of 5 μg mL^{-1} for 4 h. Before laser irradiation, the nanoparticle-containing medium was replaced with pure medium. The cells were stained with DAPI (1 μg mL^{-1}) and Mito Tracker Deep Red (1 μg mL^{-1}) to visualize cell nuclei and mitochondria, respectively, and then fixed with 4% paraformaldehyde in PBS for 15 min. The cover glass slides were washed with PBS for three times, mounted onto a glass slide with anti-fade mounting medium (Vector Laboratories, Burlingame, CA, USA), and imaged with an Olympus FluoView FV1000 confocal microscope. The Manders' colocalization coefficients between the fluorescence signals were calculated using ImageJ, as previously reported by us.[28]

Cell Metabolism:

This was conducted using the Agilent (Santa Clara, CA, USA) Seahorse XF24 Extracellular Flux Analyzer. First, the sample cartridges were hydrated according to the manufacture's instruction prior to the assay.[22] MDA-MB-231 cells were placed in the 24-well microplates (5×10^4 cells per well) and cultured at 37 °C in a 5% CO_2 incubator for 24 h. After the cells were attached, they were incubated for another 24 h with additional 100 μL of growth medium at 37 °C under 5% CO_2 atmosphere. The cells were treated with Py@Si-TH (30 μg mL^{-1}), or Py@Si-TH-DOX (3.0 μg mL^{-1} DOX, 30 μg mL^{-1} nanoparticles) for 4 h and followed either with or without 808 nm laser irradiation for 2 min (at 1.0 W cm^{-2}). After 4 h of incubation, cells in each well were rinsed two times with 600 μL of the XF stress test medium. Then, 610 μL of glucose-depleted optimization medium was added to each well and the plate was incubated at 37 °C for 1 h prior to assay. The ECARs for all samples were measured simultaneously for 16 min to establish a baseline rate. Three agents (glucose [10 mM], oligomycin [1.0 μM], and 2-deoxy-D-glucose [2-DG; 100 mM]) were injected sequentially with a specific time gap and the ECARs were measured after each injection.

Mitochondrial Membrane Potential:

To detect mitochondrial membrane potential changes, the JC-1 dye was utilized for imaging via confocal microscopy. MDA-MB-231 cells were seeded onto collagen-coated Nunc cover glass inside 35 mm culture dishes. After 24 h, cells were washed with fresh medium and incubated with fresh medium containing Py@si-H (30 μg mL^{-1}), Py@Si-TH (30 μg mL^{-1}), or Py@Si-TH-DOX nanoparticles (30 μg mL^{-1} containing 3 μg mL^{-1} DOX) at 37 °C in a 5% CO_2 incubator for 4 h. The nanoparticle-containing medium was replaced with fresh medium before laser irradiation. After irradiation, cells were cultured for an additional 6 h. Cells were then stained with DAPI (1 μg mL^{-1}) and JC-1 (1 μg mL^{-1}) for 30 min to visualize nuclei and mitochondria, respectively. The cells were subsequently fixed with 4% paraformaldehyde in PBS for 15 min and washed with PBS for three times. The cover glasses were then mounted onto a glass slide with anti-fade mounting medium (Vector Laboratories), and imaged using an Olympus FluoView FV1000 confocal microscope. The

JC-1 dye was excited at 488 nm, and the emission peaks were at 515–545 nm (green) for the JC-1 monomer and 570–600 nm (red) for the JC-1 aggregate.

In Vitro Anticancer Efficacy:

To assess in vitro anticancer efficacy, MDA-MB-231 cells were seeded at 5000 cells in 100 μL of culture medium in 96-well plate for 12 h. They were then washed with fresh medium and incubated with fresh medium containing free DOX (3 μg mL^{-1}), Py@Si-TH (30 μg mL^{-1}), Py@Si-H-DOX (30 μg mL^{-1}, containing 3 μg mL^{-1} DOX), or Py@Si-TH-DOX nanoparticles (30 μg mL^{-1}, containing 3 μg mL^{-1} DOX) at 37 °C in a 5% CO_2 incubator for 4 h. The nanoparticle-containing medium was replaced with fresh medium, followed with or without NIR laser irradiation at 1 W cm^{-2} for 2 min. Afterward, cells were cultured for an additional 44 h. Cell viability assay was conducted by using the CCK-8 according to the manufacturer's instructions.

Nanoparticle Stability in Human Blood:

Human blood samples were obtained from three healthy donors at the University of Maryland Marlene and Stewart Greenebaum Comprehensive Cancer Center (UMGCCC). The protocol (GCC 1403) for obtaining the whole blood samples was approved by the Institutional Review Board at the UMGCCC. The human whole blood samples were collected in 10 mL vacutainers coated with ethylenediaminetetraacetic acid (EDTA). The samples were centrifuged at $1071 \times g$ for 15 min, to remove blood cells and obtain human blood serum (the top layer) for further use. The nanoparticle stability in the resultant human blood serum was evaluated by incubating 1 mg mL^{-1} Py@Si-TH-DOX (with HA) or Py@Si-T-DOX (without HA) nanoparticles in 10% human blood serum (diluted with 1× PBS buffer) for 12 h at 37 °C, followed by measuring the size distribution of the nanoparticles with the DLS instrument.

Animals and Xenograft Tumor Model:

Six-week-old NU/NU nude mice were purchased from Charles River (Wilmington, MA, USA) and maintained on a 16:8 h light-dark cycle. All procedures for animal use were approved by the Institutional Animal Care and Use Committee (IACUC) at the Ohio State University (# 2011A00000059-R2) and all efforts were made to minimize animal suffering. To obtain xenograft tumors, MDA-MB-231 cells in 100 μL of mixture of PBS and Matrigel (1:1) at 10^7 cells mL^{-1} were injected subcutaneously at the dorsal side of the upper hindlimb of each 7-week-old mouse. The growth of tumors was then monitored every 2 days and the tumor volume was calculated as $V = (L \times W^2) \times 0.5$, where L is long diameter and W is short diameter of the tumors measured using a caliper.

In Vivo Photothermal Effect:

After cancer cell injection and tumor establishment for 10 days, mice bearing MDA-MB-231 tumors (≈250 mm^3) were injected intravenously with saline, free DOX (2.5 mg kg^{-1} body weight), or Py@Si-TH-DOX (25 mg kg^{-1} body weight). At 8 h and 24 h after the injection, tumors were subjected to the NIR laser irradiation at 1.0 W cm^{-2} for 1 min. During the exposure to laser, a time series of thermographic images were captured with a

FLIR E6 thermal camera at a time interval of 20 s over 1 min. The temperature of the tumor was calculated using the FLIR R&D software.

In Vivo Imaging and Biodistribution:

Mice bearing MDA-MB-231 tumors ($\approx$250 mm^3) were injected intravenously via the tail vein with either 100 μL of saline, ICG (25 μg) in 100 μL of saline, or Py@Si-TH-ICG (25 μg of ICG, the Py@Si-TH-ICG nanoparticles were made in the same way as Py@Si-TH-DOX nanoparticles by replacing DOX with ICG[2b] instead of DOX) in 100 μL of saline after the tumor reached ~250 mm^3 in long diameter. The images were taken at 2, 8, and 24 h after injection using a Perkin Elmer IVIS whole animal imaging system with an 831 nm ICG-filter to collect the fluorescence emission of ICG under 780 nm excitation. The mice were sacrificed after the whole animal imaging experiment, and tumor and major organs were harvested for ex vivo fluorescence imaging using the same IVIS system.

In Vivo Antitumor Efficacy:

Mice bearing MDA-MB-231 tumors ($\approx$250 mm^3) were injected intravenously via the tail vein with either 100 μL of saline or the same amount of saline containing Py@Si-TH nanoparticles, Py@Si-TH-DOX nanoparticles, free DOX (with NIR laser irradiation), Py@Si-TH nanoparticles (with NIR laser irradiation), Py@Si-H-DOX nanoparticles (with NIR laser irradiation), or Py@Si-TH-DOX (with NIR laser irradiation). The DOX dose was 2.5 mg kg^{-1} body weight, and the nanoparticle dose was 25 mg kg^{-1} body weight. The NIR laser irradiation was applied at 8 h and 24 h for 1 min each after the intravenous injection. Tumor growth and body weight were monitored every 2 days. The number of animals in each group ($n = 7$) was chosen to ensure statistical significance of the experimental data. The mice were euthanized at day 29 after the injection. Tumors, livers, lungs, hearts, spleens, and kidneys were collected, formalin-fixed, paraffin-embedded, and H&E stained for further histological analysis.

Statistical Analysis:

All data were reported as mean ± standard deviation (s.d.) from at least three independent experiments. Student's t-test (unpaired and two-tailed) was used to compare two groups of independent samples. One-way analysis of variance (ANOVA) with Dunnett's post hoc analysis was used for comparison among more than two groups. In all cases, a $p < 0.05$ was considered to be statistically significant. All statistical analyses were carried out with GraphPad Prism 7.0 (San Diego, CA, USA).

Supplementary Material

Refer to Web version on PubMed Central for supplementary material.

Acknowledgements

# References

[1]. a)Mayer EL, Burstein HJ, J. Clin. Oncol 2016, 34, 3369; [PubMed: 27551109] b)Denkert C, Liedtke C, Tutt A, von Minckwitz G, Lancet 2017, 389, 2430. [PubMed: 27939063]

[2]. a)Miller KD, Siegel RL, Lin CC, Mariotto AB, Kramer JL, Rowland JH, Stein KD, Alteri R, Jemal A, Cancer J Clin. 2016, 66, 271;b)Wang H, Agarwal P, Zhao S, Yu J, Lu X, He X, Nat. Commun 2015, 6, 10081; [PubMed: 26621191] c)Oualla K, El-Zawahry HM, Arun B, Reuben JM, Woodward WA, Gamal El-Din H, Lim B, Mellas N, Ueno NT, Fouad TM, Ther. Adv. Med. Oncol 2017, 9, 493; [PubMed: 28717401] d)Schettini F, Giuliano M, De Placido S, Arpino G, Cancer Treat. Rev 2016, 50, 129; [PubMed: 27665540] e)Locatelli MA, Curigliano G, Eniu A, Breast Care 2017, 12, 152; [PubMed: 28785182] f)Yao H, He G, Yan S, Chen C, Song L, Rosol TJ, Deng X, Oncotarget 2017, 8, 1913; [PubMed: 27765921] g)Zeichner SB, Terawaki H, Gogineni K, Breast Cancer 2016, 10, 25. [PubMed: 27042088]

[3]. Dean M, Fojo T, Bates S, Nat. Rev. Cancer 2005, 5, 275. [PubMed: 15803154]

[4]. a)Blanco E, Shen H, Ferrari M, Nat. Biotechnol 2015, 33, 941; [PubMed: 26348965] b)Sherlock SP, Tabakman SM, Xie L, Dai H, ACS Nano 2011, 5, 1505; [PubMed: 21284398] c)Langer R, Science 249, 1990, 1527; [PubMed: 2218494] d)Farokhzad OC, Langer R, ACS Nano 2009, 3, 16; [PubMed: 19206243] e)Hare JI, Lammers T, Ashford MB, Puri S, Storm G, Barry ST, Adv. Drug Delivery Rev 2017, 108, 25;f)Wilhelm S, Tavares AJ, Dai Q, Ohta S, Audet J, Dvorak HF, Chan WCW, Nat. Rev. Mater 2016, 1, 16014.

[5]. a)Kamaly N, Yameen B, Wu J, Farokhzad OC, Chem. Rev 2016, 116, 2602; [PubMed: 26854975] b)Masoud H, Alexeev A, ACS Nano 2012, 6, 212; [PubMed: 22176274] c)Slowing II, Vivero-Escoto JL, Wu C-W, Lin VS-Y, Adv. Drug Delivery Rev 2008, 60, 1278.

[6]. a)Lin Q, Huang Q, Li C, Bao C, Liu Z, Li F, Zhu L, J. Am. Chem. Soc 2010, 132, 10645; [PubMed: 20681684] b)Yavuz MS, Cheng Y, Chen J, Cobley CM, Zhang Q, Rycenga M, Xie J, Kim C, Song KH, Schwartz AG, Wang LV, Xia Y, Nat. Mater 2009, 8, 935; [PubMed: 19881498] c)Huang L, Li Z, Zhao Y, Yang J, Yang Y, Pendharkar AI, Zhang Y, Kelmar S, Chen L, Wu W, Zhao J, Han G, Adv. Mater 2017, 29.

[7]. a)Xu J, Zeng F, Wu H, Wu S, J. Mater. Chem. B 2015, 3, 4904; [PubMed: 32262679] b)You J, Zhang G, Li C, ACS Nano 2010, 4, 1033; [PubMed: 20121065] c)Wang H, Agarwal P, Zhao S, Yu J, Lu X, He X, Adv. Mater 2016, 28, 347. [PubMed: 26567892]

[8]. a)Espinosa A, Di Corato R, Kolosnjaj-Tabi J, Flaud P, Pellegrino T, Wilhelm C, ACS Nano 2016, 10, 2436; [PubMed: 26766814] b)Lee J-H, Jang J.-t., Choi J.-s., Moon SH, Noh S.-h., Kim J.-w., Kim J-G, Kim I-S, Park KI, Cheon J, Nat. Nanotechnol 2011, 6, 418; [PubMed: 21706024] c)Lin L-S, Cong Z-X, Cao J-B, Ke K-M, Peng Q-L, Gao J, Yang H-H, Liu G, Chen X, ACS Nano 2014, 8, 3876; [PubMed: 24654734] d)El-Sayed IH, Huang X, El-Sayed MA, Cancer Lett. 2006, 239, 129. [PubMed: 16198049]

[9]. a)Shen Y, Zhang X, Liang L, Yue J, Huang D, Xu W, Shi W, Liang C, Xu S, Carbon 2020, 156, 558;b)Zhang B, Yu Q, Zhang Y-M, Liu Y, Chem. Commun 2019, 55, 12200;c)Ke L, Zhang C, Liao X, Qiu K, Rees TW, Chen Y, Zhao Z, Ji L, Chao H, Chem. Commun 2019, 55, 10273;d)Tan Y, Zhu Y, Wen L, Yang X, Liu X, Meng T, Dai S, Ping Y, Yuan H, Hu F, Theranostics 2019, 9, 691; [PubMed: 30809302] e)Yang X, Wang D, Zhu J, Xue L, Ou C, Wang W, Lu M, Song X, Dong X, Chem. Sci 2019, 10, 3779; [PubMed: 30996966] f)Chen S, Lei Q, Qiu W-X, Liu L-H, Zheng D-W, Fan J-X, Rong L, Sun Y-X, Zhang X-Z, Biomaterials 2017, 117, 92; [PubMed: 27939904] g)Chakrabortty S, Sison M, Wu Y, Ladenburger A, Pramanik G, Biskupek J, Extermann J, Kaiser U, Lasser T, Weil T, Biomater. Sci 2017, 5, 966; [PubMed: 28282092] h)Ju E, Li Z, Liu Z, Ren J, Qu X, ACS Appl. Mater. Interfaces 2014, 6, 4364. [PubMed: 24559457]

[10]. a)Balaban RS, Nemoto S, Finkel T, Cell 2005, 120, 483; [PubMed: 15734681] b)Green DR, Reed JC, Science 1998, 281, 1309; [PubMed: 9721092] c)Wang H, Gao Z, Liu X, Agarwal P, Zhao S, Conroy DW, Ji G, Yu J, Jaroniec CP, Liu Z, Lu X, Li X, He X, Nat. Commun 2018, 9, 562. [PubMed: 29422620]

[11]. a)Fulda S, Galluzzi L, Kroemer G, Nat. Rev. Drug Discovery 2010, 9, 447; [PubMed: 20467424] b)Murphy MP, Smith RAJ, Annu. Rev. Pharmacol. Toxicol 2007, 47, 629. [PubMed: 17014364]

[12]. Sarosiek KA, Chonghaile TN, Letai A, Trends Cell Biol. 2013, 23, 612. [PubMed: 24060597]

[13]. a)Xu J, Zeng F, Wu H, Hu C, Wu S, Biomacromolecules 2014, 15, 4249; [PubMed: 25329523] b)Shah BP, Pasquale N, De G, Tan T, Ma J, Lee K-B, ACS Nano 2014, 8, 9379. [PubMed: 25133971]

[14]. a)Banerji S, Wright AJ, Noble M, Mahoney DJ, Campbell ID, Day AJ, Jackson DG, Nat. Struct. Mol. Biol 2007, 14, 234; [PubMed: 17293874] b)Wang H, Agarwal P, Zhao S, Xu RX, Yu J, Lu X, He X, Biomaterials 2015, 72, 74; [PubMed: 26344365] c)Wang H, Agarwal P, Zhao S, Yu J, Lu X, He X, Biomaterials 2016, 97, 62. [PubMed: 27162075]

[15]. a)Smith RAJ, Porteous CM, Gane AM, Murphy MP, Proc. Natl. Acad. Sci. U. S. A 2003, 100, 5407; [PubMed: 12697897] b)Kwon HJ, Cha M-Y, Kim D, Kim DK, Soh M, Shin K, Hyeon T, Mook-Jung I, ACS Nano 2016, 10, 2860; [PubMed: 26844592] c)Yu H, Jin F, Liu D, Shu G, Wang X, Qi J, Sun M, Yang P, Jiang S, Ying X, Du Y, Theranostics 2020, 10, 2342. [PubMed: 32104507]

[16]. a)Tong S, Quinto CA, Zhang L, Mohindra P, Bao G, ACS Nano 2017, 11, 6808; [PubMed: 28625045] b)Laurent S, Forge D, Port M, Roch A, Robic C, Vander Elst L, Muller RN, Chem. Rev 2008, 108, 2064. [PubMed: 18543879]

[17]. a)Liu H, Chen D, Li L, Liu T, Tan L, Wu X, Tang F, Angew. Chem., Int. Ed 2011, 50, 891;b)Huang X, El-Sayed IH, Qian W, El-Sayed MA, J. Am. Chem. Soc 2006, 128, 2115. [PubMed: 16464114]

[18]. a)Zha Z, Yue X, Ren Q, Dai Z, Adv. Mater 2013, 25, 777; [PubMed: 23143782] b)Yang K, Xu H, Cheng L, Sun C, Wang J, Liu Z, Adv. Mater 2012, 24, 5586. [PubMed: 22907876]

[19]. Whatcott CJ, Han H, Posner RG, Hostetter G, Von Hoff DD, Cancer Discov. 2011, 1, 291. [PubMed: 22053288]

[20]. a)He X, Bischof JC, Crit. Rev. Biomed. Eng 2003, 31, 355; [PubMed: 15139301] b)He X, Open Biomed. Eng. J 2011, 5, 47. [PubMed: 21769301]

[21]. a)Marrache S, Dhar S, Proc. Natl. Acad. Sci. U. S. A 2012, 109, 16288; [PubMed: 22991470] b)Wang H, Feng Z, Wang Y, Zhou R, Yang Z, Xu B, J. Am. Chem. Soc 2016, 138, 16046. [PubMed: 27960313]

[22]. Marrache S, Dhar S, Chem. Sci 2015, 6, 1832. [PubMed: 25709804]

[23]. Xu R.-h., Pelicano H, Zhou Y, Carew JS, Feng L, Bhalla KN, Keating MJ, Huang P, Cancer Res. 2005, 65, 613. [PubMed: 15695406]

[24]. a)Calmettes G, John SA, Weiss JN, Ribalet B, J. Gen. Physiol 2013, 142, 425; [PubMed: 24081983] b)Liberti MV, Locasale JW, Trends Biochem. Sci 2016, 41, 211; [PubMed: 26778478] c)Weinberg SE, Chandel NS, Nat. Chem. Biol 2015, 11, 9. [PubMed: 25517383]

[25]. Wang H, Yu J, Lu X, He X, Nanomedicine 2016, 11, 103. [PubMed: 26653177]

[26]. a)Sindhwani S, Syed AM, Ngai J, Kingston BR, Maiorino L, Rothschild J, MacMillan P, Zhang Y, Rajesh NU, Hoang T, Wu JLY, Wilhelm S, Zilman A, Gadde S, Sulaiman A, Ouyang B, Lin Z, Wang L, Egeblad M, Chan WCW, Nat. Mater 2020, 19, 566; [PubMed: 31932672] b)de Lazaro I, Mooney DJ, Nat. Mater 2020, 19, 486; [PubMed: 32332989] c)Pandit S, Dutta D, Nie S, Nat. Mater 2020, 19, 478. [PubMed: 32332990]

[27]. a)Hong J-Y, Yoon H, Jang J, Small 2010, 6, 679; [PubMed: 20127667] b)Wang M, Polymers 2016, 8, 373.

[28]. Xu J, Liu Y, Li Y, Wang H, Stewart S, Van der Jeught K, Agarwal P, Zhang Y, Liu S, Zhao G, Wan J, Lu X, He X, Nat. Nanotechnol 2019, 14, 388. [PubMed: 30804480]
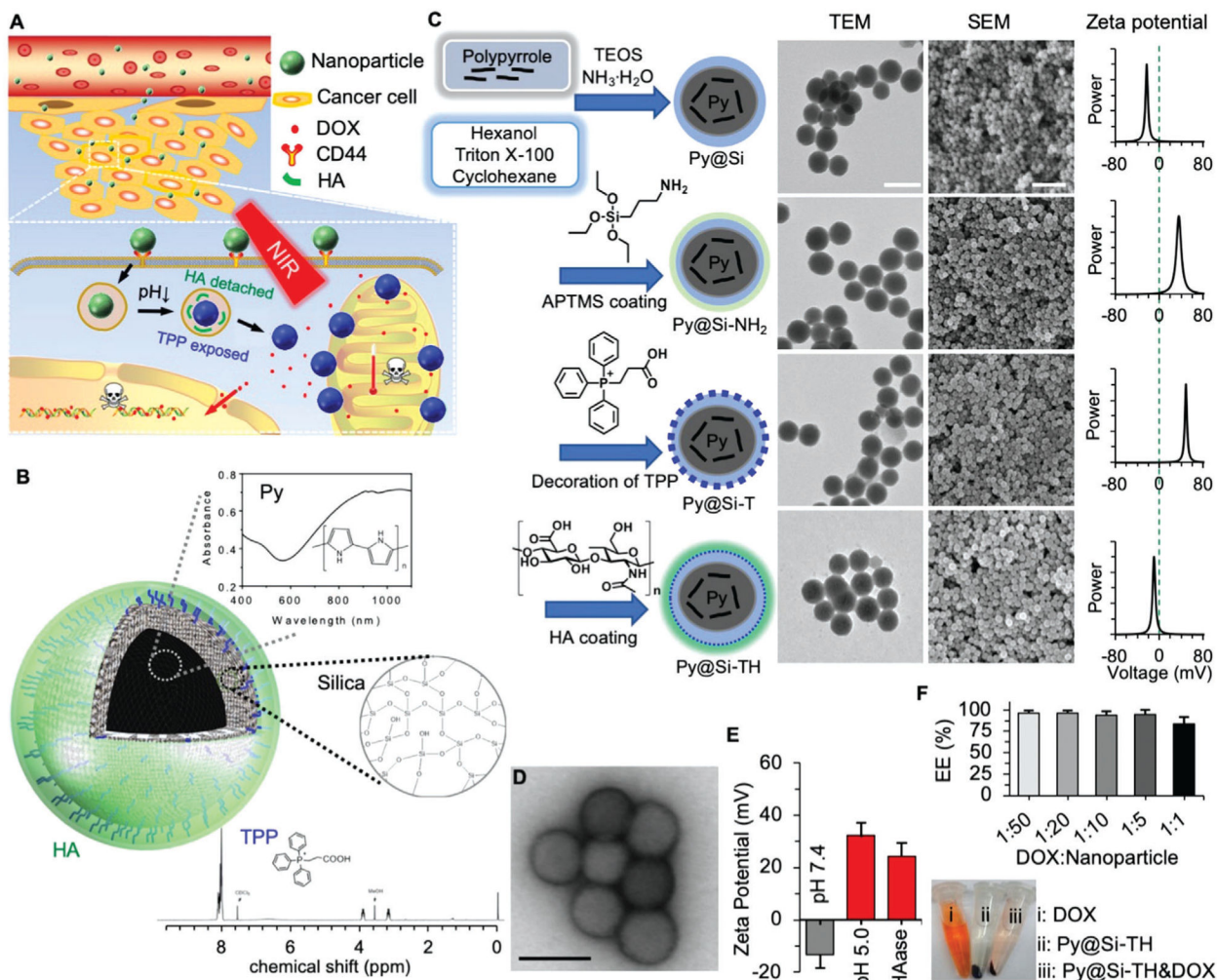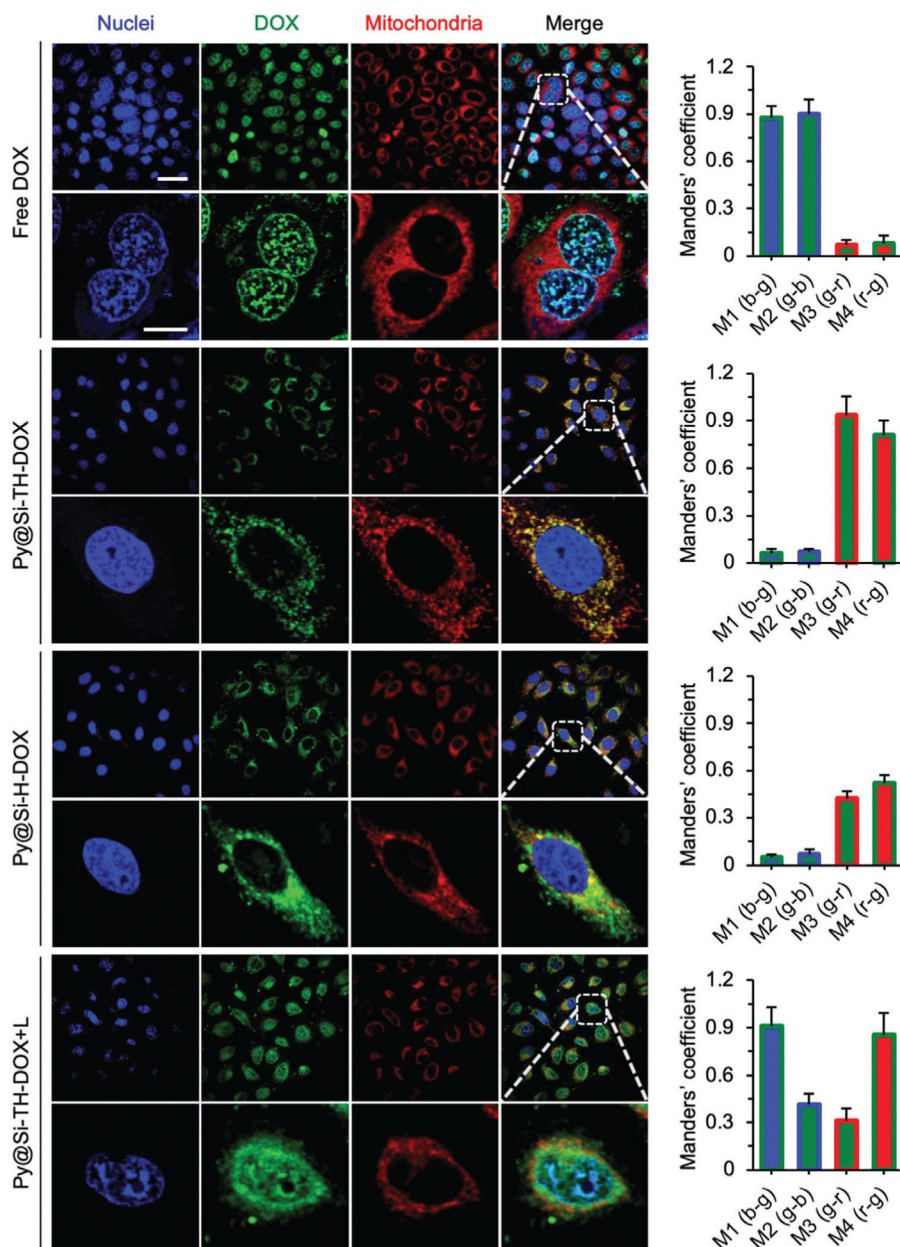
Figure 1.
Synthesis and characterization of nanoparticles. A) A schematic illustration of the nanoparticle in targeting tumor via the enhanced permeability and retention (EPR) effect of tumor vasculature, cancer cells via CD44, and mitochondria via triphenylphosphonium (TPP) for chemo-photothermal therapy of cancer. B) A schematic illustration of the structure of the nanoparticle together with materials in the nanoparticles. Py: polypyrrole. HA: hyaluronic acid. C) The procedure for preparing Py-embedded silica (Py@Si) nanoparticles, modifying the Py@Si nanoparticles with (3-aminopropyl) trimethoxysilane (APTMS) to form Py@Si-NH$_2$ nanoparticles, coating the Py@Si-NH$_2$ nanoparticles with TPP to produce mitochondria-targeting Py@Si-T nanoparticles, and finally, coating the Py@Si-T nanoparticles with HA to produce Py@Si-TH nanoparticles. Transmission electron microscopy (TEM) and scanning electron microscopy (SEM) images were also given to show the morphology of the nanoparticles. The difference in surface zeta potential of the Py@Si, Py@Si-NH$_2$, Py@Si-T, and Py@Si-TH nanoparticles demonstrating the successful sequential modification of the positively charged APTMS and TPP and negatively charged HA on the nanoparticle surface. Scale bar: 100 and 500 nm for the TEM and SEM images, respectively. D) TEM images of Py@Si-TH nanoparticles with negative staining showing

the HA coating on the outermost surface of the nanoparticles. Scale bar: 100 nm). E) Zeta potential data showing HA detachment from Py@Si-TH nanoparticles after treatment at low pH or with hyaluronidase (HAase). All the zeta potential data were measured by redispersing the nanoparticles in deionized water at neutral pH after the treatments. F) Encapsulation efficiency (EE) of doxorubicin hydrochloride (DOX) by simply mixing it with Py@Si-TH nanoparticles at different feeding ratios (DOX:nanoparticle in weight) for 1 h. Centrifuge tubes depicting the color of DOX, Py@Si-TH nanoparticles, and mixture of DOX and Py@Si-TH nanoparticles (1:1) after centrifuging (13 000 × *g*), indicating the high EE of DOX with the nanoparticles at the high feeding ratio.
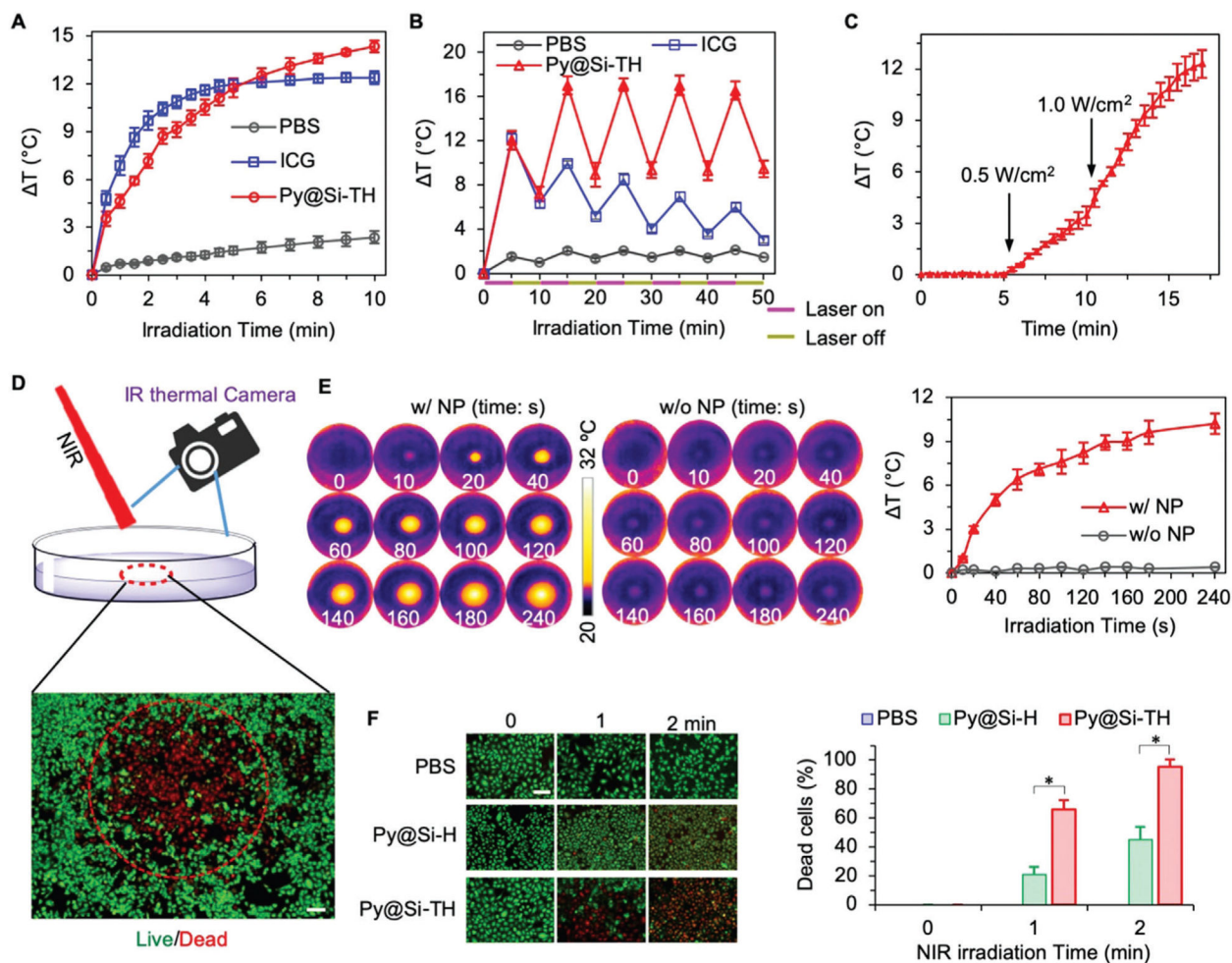
Figure 2.
Photothermal effect of nanoparticles. A) Increase in temperature of phosphate buffered saline (PBS) and PBS suspended/dissolved with Py@Si-TH nanoparticles (30 μg mL^{-1}) or free ICG (5 μg mL^{-1}) upon NIR laser irradiation at 1.0 W cm^{-2}. B) Photothermal effect of Py@Si-TH nanoparticles versus ICG in PBS with five cycles of on/off NIR laser irradiation, showing excellent photothermal stability of the nanoparticles compared to ICG. C) Laser power density dependent photothermal effect of Py@Si-TH nanoparticles, showing different temperature increasing rates from 0.5 to 1.0 W cm^{-2}. D) A schematic diagram showing MDA-MB-231 cells in a dish treated with Py@Si-TH nanoparticles upon NIR laser irradiation. The red circle shows the area of irradiation. The local temperature change was monitored by an FLIR E6 infrared (IR) thermal camera. Cells were stained with calcein AM and propidium iodide (PI) to fluorescently visualize the live/dead information after laser irradiation. Scale bar: 200 μm. E) IR thermal images of MDA-MB-231 cells with (w/ NP) or without (w/o NP) Py@Si-TH nanoparticles upon laser irradiation, and the corresponding curves of temperature change. F) Fluorescence microscopy images showing live/dead (green/red) cells and the percentage of dead cells (the number of PI positive cells to the total number of cells) after treating MDA-MB-231 cells with PBS, Py@Si-H nanoparticles, and Py@Si-TH nanoparticles in combination with laser irradiation for 0, 1, or 2 min. Statistical

significance was assessed by Student's t-test (unpaired and two-tailed); $n = 3$; and scale bar: 50 μm. $*p < 0.05$.
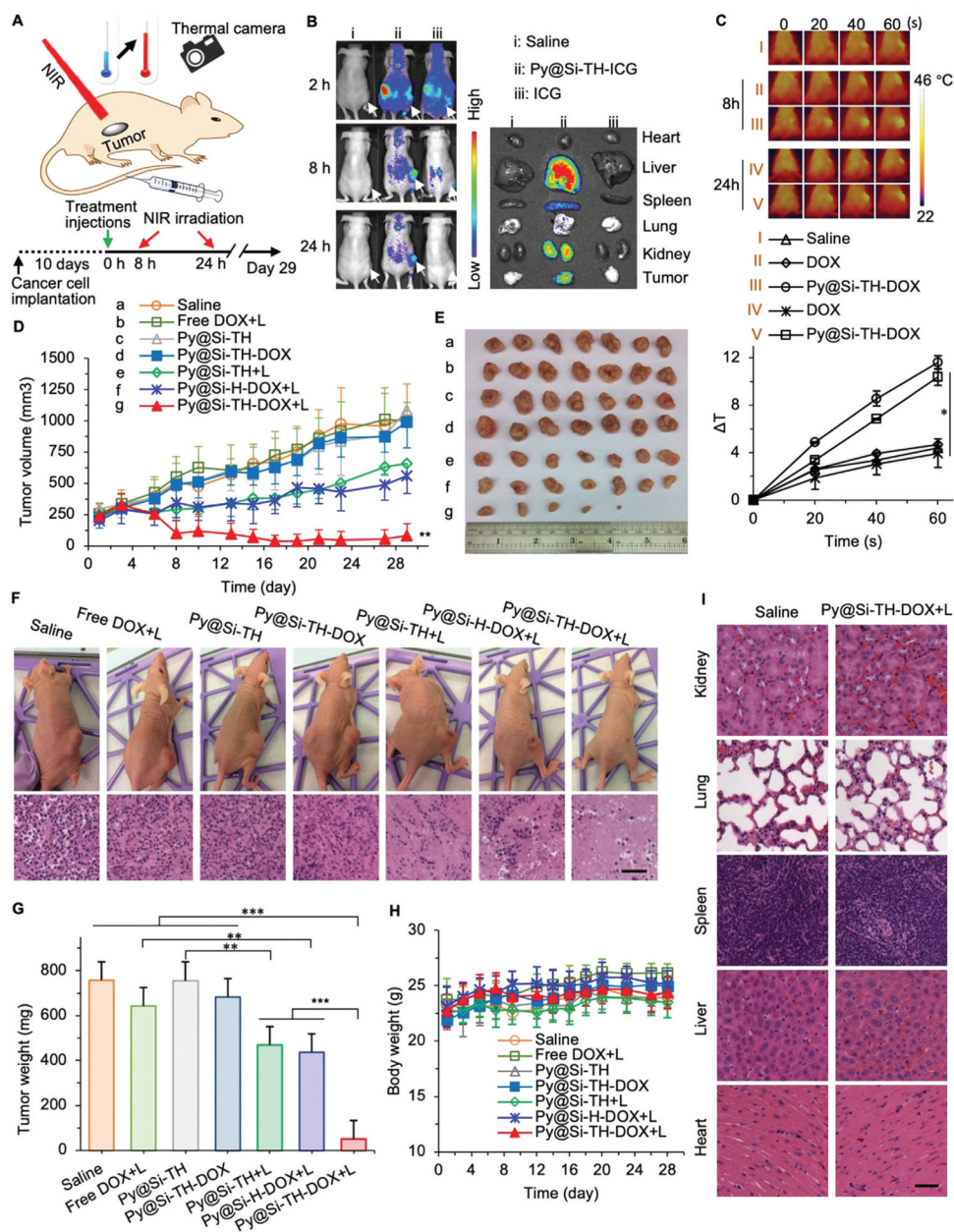
Figure 3.
Cell uptake of nanoparticles and their subcellular distribution. Confocal images showing cell uptake and subcellular distribution of Py@Si-TH-DOX nanoparticles compared with free DOX and Py@Si-H-DOX nanoparticles (no mitochondria targeting capability) in MDA-MB-231 cells. Cells were incubated with MitoTracker Deep Red (red) and DAPI (blue) to stain their mitochondria and nuclei, respectively. The merged and zoom-in images show effective overlap of mitochondria (red) and the Py@Si-TH-DOX nanoparticles (green), demonstrating the mitochondria-targeting capability of the nanoparticles. Such overlap is minimal for the Py@Si-H-DOX nanoparticles. Furthermore, the overlap between cell nuclei (blue) and DOX (green) is evident after NIR laser irradiation of the cells treated with Py@Si-TH-DOX nanoparticles (i.e., Py@Si-TH-DOX+L), because of the high binding

affinity between DOX and the nuclear materials. This indicates the NIR laser-triggered release of DOX from the nanoparticles inside cells. These qualitative observations are confirmed by quantitative analyses of the colocalization of DOX with nuclei and mitochondria using Manders' coefficients: M1 (b–g) denotes the fraction of nuclei/blue overlapping with DOX/green, M2 (g–b) denotes the fraction of DOX/green overlapping with nuclei/blue, M3 (g–r) denotes the fraction of DOX/green overlapping with mitochondria/red, and M4 (r–g) denotes the fraction of mitochondria/red overlapping with DOX/green. Scale bars: 20 μm and 5 μm for low and high magnification images, respectively.
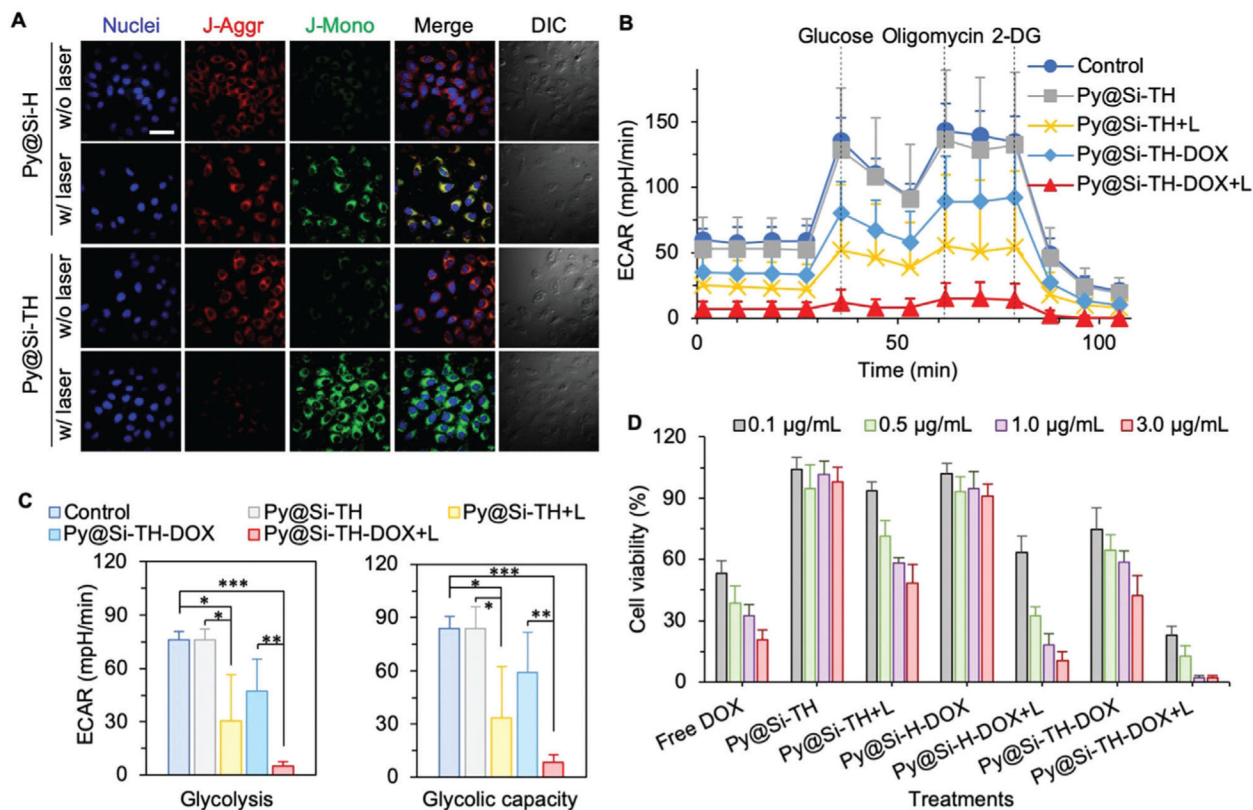
Figure 4.
Mitochondrial damage analyses and in vitro anticancer efficacy. A) Mitochondrial membrane potential of MDA-MB-231 cells loaded with Py@Si-TH (with mitochondria targeting) versus Py@Si-H (without mitochondria targeting) nanoparticles with or without laser irradiation, indicating enhanced mitochondrial damage with Py@Si-TH nanoparticles under NIR laser irradiation. Scale bar: 20 μm. B) Real-time extracellular acidification rate (ECAR) analysis of MDA-MB-231 cells either without any treatment (control) or after treated with Py@Si-TH, Py@Si-TH+L (L: NIR laser irradiation), Py@Si-TH-DOX, and Py@Si-TH-DOX+L. 2-DG: 2-deoxy-D-glucose. C) Comparison of glycolysis and glycolytic capacity (the summation of glycolysis and glycolytic reserve) of the cells with different treatments. Statistical significance was assessed by Student's t-test (unpaired and two tailed); $n = 3$; and $*p < 0.05$, $**p < 0.01$, $***p < 0.001$. D) Targeted heating of mitochondria augments chemotherapy in vitro. The MDA-MB-231 cells were greatly sensitized to nanoparticle-mediated chemotherapy after targeted heating (+L) of mitochondria.

Figure 5.

In vivo tumor targeting and antitumor efficacy and safety. A) A schematic diagram of the in vivo experiment showing tumor-bearing mice were injected with various drug formulations including the Py@Si-TH-DOX nanoparticles intravenously via the tail vein followed by NIR laser irradiation (+L for some mice), together with a sketch describing the exact timing according to which the injections/treatments of the mice were performed from the implantation of cancer cells. Temperature change in the tumor area was monitored with an IR thermal camera. B) In vivo whole animal imaging of ICG fluorescence at 2, 8, and 24 h after intravenous injection of saline, Py@Si-TH-ICG nanoparticles (i.e., Py@Si-TH nanoparticles encapsulated with ICG), or free ICG, showing effective tumor targeting of the Py@Si-TH nanoparticles. The arrows indicate the locations of tumors in mice. Also shown

is the ex vivo imaging of tumors and critical organs collected from the mice sacrificed at 24 h, confirming the tumor targeting capability of the Py@Si-TH nanoparticle observed with whole animal imaging. C) IR thermal images (top) of mice injected with free DOX or Py@Si-TH-DOX nanoparticles upon laser irradiation for various time periods (0–60 s) at 8 h and 24 h after the injections. Saline was used as control. The corresponding heating curves (bottom) show the significantly increased temperature in tumor for the group of Py@Si-TH-DOX upon NIR laser irradiation. Error bars represent s.d. ($n = 3$). D) Tumor growth and E) a photo of the tumors collected on day 29 after sacrificing the mice. F) Photos of representative mice on day 29 for the seven different treatments, together with representative images of the histology (Hematoxylin&eosin or H&E stain) of the tumors from mice for the seven treatments. G) Weight of the tumors collected after sacrificing the mice on day 29. H) Body weight of the mice with the various treatments showing no significant change for the mice with the seven treatments. I) Histological (H&E) images of five major organs in mice treated with saline or Py@Si-TH-DOX+L collected on day 29. All NIR laser irradiation was administered at 1.0 W cm^{-2} for 1 min. The NIR irradiation were conducted at 8 h and 24 h after intravenous administration of the various treatments. Statistical significance was assessed by Student t-test when comparing two groups (G), and one-way ANOVA with a Fisher's least significant difference (LSD) post hoc test (C,D) or a Dunnett's post hoc test (G) when comparing more than two groups; error bars represent s.d. ($n = 7$); scale bars: 50 μm; and $*p < 0.05$, $**p < 0.01$.